Geophysical Journal International

Geophys. J. Int. (2017) **211,** 93–106
Advance Access publication 2017 July 14
GJI Seismology

doi: 10.1093/gji/ggx292

An $M_w = 7.7$ slow earthquake in 1960 near the Aysén Fjord region, Chile

Hiroo Kanamori[1] and Luis Rivera[2]

[1] *Seismological Laboratory, California Institute of Technology, Pasadena, CA* 91125, *USA. E-mail: hiroo@gps.caltech.edu*
[2] *Institut de Physique du Globe de Strasbourg (UMR*7516*), Université de Strasbourg, CNRS, F-*67084 *Strasbourg, France*

Accepted 2017 July 12. Received 2017 July 3; in original form 2017 March 15

SUMMARY

We re-examine the source characteristics of an $M_s = 6.9$ earthquake in Chile which occurred on 1960 June 6, near the Aysén Fjord region where a remarkable earthquake swarm occurred in 2007 with more than 7000 earthquakes and hundreds of landslides. The June 6 event occurred during the aftershock activity of the 1960 May 22, $M_w = 9.5$ great Chilean earthquake. A recently found well-calibrated strain seismogram of the June 6 event recorded at Isabella (ISA), California, is the impetus to this study. We confirm that this event is a slow earthquake caused by a source process extending at least 190 s with a seismic moment of $M_0 = 4.5 \times 10^{20}$ N·m ($M_w = 7.7$). Although the mechanism cannot be uniquely determined, an NS trending right-lateral strike-slip mechanism is consistent with the ISA record. The depth cannot be constrained well, but the slowness of the event suggests that it may have occurred in a somewhat deeper high-temperature ductile environment caused by nearby subduction of the Chile Rise. The mechanism and the proximity of this event to the Liquiñe-Ofqui fault (LOF) which extends north–south over 1000 km along the Chilean coast suggest that the June 6 event represents a slip on this fault. The large moment of the June 6 event indicates strong interaction between the Nazca-South American plate boundary and the LOF with significant slip partitioning.

Key words: South America; Earthquake dynamics; Earthquake source observations; Surface waves and free oscillations; Dynamics and mechanics of faulting.

1 INTRODUCTION

A remarkable earthquake swarm with more than 7000 recorded events, hundreds of landslides and local tsunamis occurred in 2007 in the Aysén Fjord area in Chile (e.g. Comte *et al.* 2007; Naranjo *et al.* 2009; Sepulveda *et al.* 2010, Fig. 1). Because of its regional seismic hazard implication and the unique tectonic environment associated with subduction of the Chile Rise, it attracted the attention of many investigators. The swarm began 2007 January 23, and the largest earthquake, $M_w = 6.2$, occurred on 2007 April 21 (17:53:48.3 UT, $M_w = 6.2$, $M_0 = 2.8 \times 10^{18}$ N·m, Lat. $= -45.48°$, Long. $= -72.95°$ and depth $= 12$ km). The swarm activity is generally considered to be associated with tectonic activity along the NS trending right-lateral Liquiñe Ofqui fault (LOF) which extends over 1200 km along the Chilean coast (Fig. 1, Sepulveda & Serey 2009; Sepulveda *et al.* 2010; Legrand *et al.* 2011; Agurto *et al.* 2012; Perez-Flores *et al.* 2016). For the period from 1976 January 1 to 2016 December 31, the Global Centroid Moment Tensor (GCMT) catalogue lists nine earthquakes with M_w ranging from 5.0 to 6.2 within the area bounded by ($-46°$ to $-44°$) in latitude and ($-74°$ to $-72°$) in longitude (Figs 1 and 2). The mechanisms of these nine earthquakes vary considerably, but they are roughly either NS striking right-lateral or EW striking left-lateral strike-slip. The mechanism of the largest event on April 21 has a large non-double-couple (NDC) component with the best double couple (DC) given by strike/dip/rake (s/d/r) $= 84°/86°/2°$ or $354°/88°/176°$ (Fig. 2). In the following, we call the GCMT mechanism with the NDC component, AM-1 and the DC mechanism s/d/r $= 84°/86°/2°$, A-1. Agurto *et al.* (2012) made a detailed study of the locations and mechanisms of the swarm earthquakes.

Prior to this swarm activity, the seismicity in this region had been poorly known. Gutenberg & Richter (1954) lists an $M_{G\text{-}R} = 7.1$ earthquake at $-44.5°$ and $-73°$ in 1927 (Fig. 1, November 21, 23:12:25UT). Very little is known about this earthquake. Chinn & Isacks (1983) list an earthquake with $M_s = 6.1$ (Fig. 1, November 28, 1965, 03:56UT) at $-45.77°$ and $-72.90°$ (depth $= 33$ km, Naranjo *et al.* 2009). The mechanism of this event determined by Chinn & Isacks (1983) is primarily strike-slip similar to those of the larger Aysén swarm earthquakes in 2007.

During the aftershock sequence of the 1960 May 22, $M_w = 9.5$ Chilean earthquake (hereafter referred to as the May 22 event), an $M_s = 6.9$ (Rothé 1969) aftershock occurred in this region on 1960 June 6 (Fig. 1, 05:55:49.1UT, $-45.7°$. $-73.502°$ and depth $= 15$ km). Hereafter, this event is referred to as the June 6 event. According to Cifuentes (1989), this is probably the largest aftershock of the May 22 event during 1 yr after the main shock. Despite the large magnitude, it has not received much attention probably because it occurred during the aftermath of the May 22 event (Barrientos, private communication, 2013). Kanamori & Stewart (1979) noted long-period multiple Love (G3 and G4) and Rayleigh

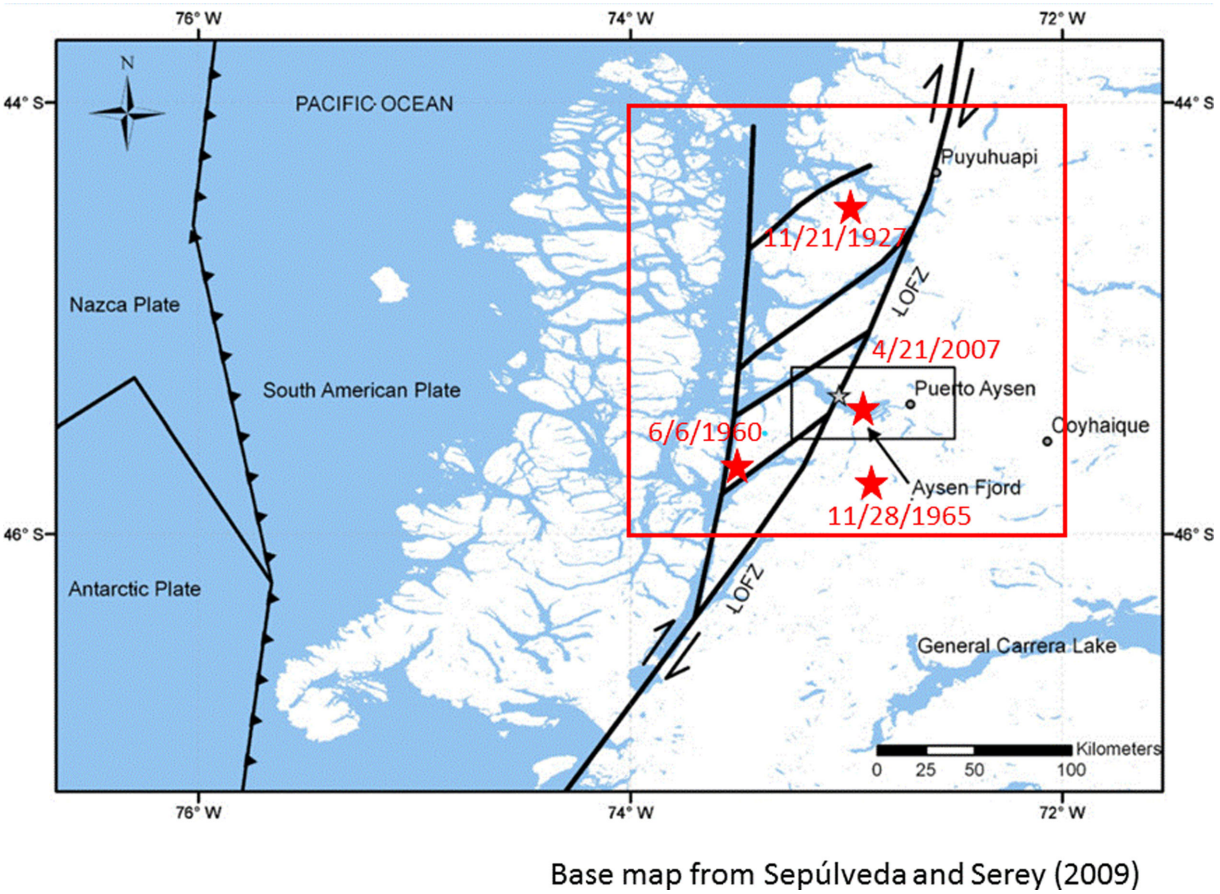

Figure 1. Aysén Fjord area (black box) and the epicentres of the 1960 June 6, 2007 April 21, 1927 November 21 and 1965 November 28 earthquakes. LOFZ indicates the Liquiñe Ofqui fault zone. Red box is the area which includes nine earthquakes for which the Global Centroid Moment Tensor (GCMT) mechanisms are available.

(R3 and R4) waves on Press–Ewing seismograms recorded at Pasadena, California and Ruth, Nevada, and found that amplitudes of G3, G4, R3 and R4 waves were much larger than normally expected for an $M_s = 6.9$ event. They estimated the seismic moment as 5.6×10^{20} N·m ($M_w = 7.8$). With very limited and ambiguous first-motion data, Kanamori and Stewart chose a solution s/d/r $= 80°/90°/196°$ with the assumption that it occurred on the extension of a transform fault of the Chile Rise, but the mechanism was poorly constrained and tentative.

Now, with the much better understanding of the Aysén earthquake swarm thanks to the many recent studies and the availability of many GCMT mechanism solutions for the area, we revisit this earthquake. Recently, Prof. Stewart Smith provided us with the original strip-chart record of the Benioff strain seismogram of the May 22, event recorded at Isabella (ISA), California. The record is not the direct strain record shown by fig. 13 of Benioff (1962). The signal from the direct strain record was passed through a capacitor– resistor (CR) network to enhance the response to the Earth's free oscillations and long-period surface waves by suppressing the tidal signal. The first reliable measurements of Earth's free oscillations were made by Benioff *et al.* (1961) from this record. This is a continuous record covering the period from 21:00 UT, 1960 May 27 to June 9. Toward the end of this long record, physically about 48 m long, we found the 1960 June 6 event recorded with clear S, G1, R1, G2 and R2 phases (Fig. 3a). On this strip-chart record. the June 6 event is the largest aftershock during the period from 1960 May 27 to June 9.

With a detailed analysis of this record together with the direct ISA strain record for the May 22 event (Benioff 1962), we could calibrate this record accurately (Appendix). This record is far more reliable and better calibrated than the data available to Kanamori & Stewart (1979), especially at long period, and motivated us to make a more detailed examination of the June 6 event.

2 MECHANISM

For the June 6 earthquake, in addition to the ISA strain record, the International Geophysical Year (IGY)-type long-period records at Tsukuba (TSK), Japan, a Benioff direct strain record (N29°W component) at Ñaña (NNA), Peru and Press–Ewing seismograms at PAS are available. Since the quality of the ISA strain record is far better than the other records, we primarily use it, while the TSK and NNA records are used only for checking some details.

The record shown in Fig. 3(a) is the output from a CR network connected to the displacement transducer at one end of the extensometer. The response of the CR network together with our calibration is shown in Fig. 3(b). Note that the peak response is at 1987 s.

We first compute synthetic seismograms using the best DC mechanism of the 2007 April 21, $M_w = 6.2$ Aysén earthquake shown in Fig. 2 (A-1 mechanism). We compute the strain (extension in the strain-rod direction) by numerically differencing the displacements at two endpoints along the strain rod. Then, we convolve it with the network response, and apply a filter representing the

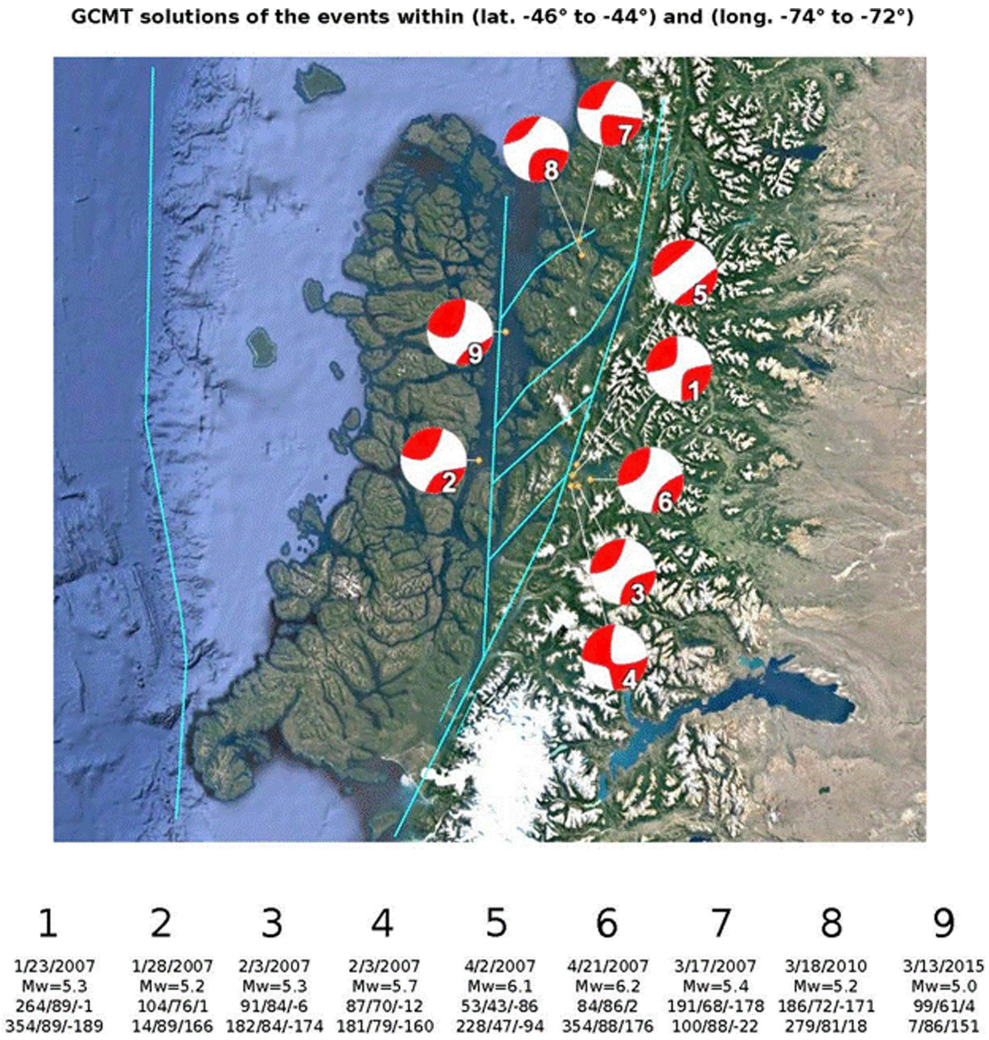

Figure 2. GCMT mechanisms of the earthquakes near the Aysén Fjord area (red box in Fig. 1). The 2007 April 21 event is the largest event with $M_w = 6.2$. The GCMT mechanism and its best double-couple mechanism are referred to as AM-1 and A-1. The A-1 mechanism is strike/dip/rake (s/d/r) = 84°/86°/2°. (The base map is taken from Google Earth.)

long-period source characteristics. We use two methods for computing the synthetic displacement records. First, we employ the normal-mode summation method using the mode catalogue built with the program MINOS (Woodhouse 1988) along with the PREM Earth's model (Dziewonski & Anderson 1981). Second, we use the IRIS (Incorporated Research Institutions for Seismology) Synthetics Engine (Syngine, IRIS URL https://service.iris.edu/irisws/syngine/, last accessed 20 July 2017). The Green's functions are pre-computed with the AxiSEM (Nissen-Meyer *et al.* 2014) for several 1-D reference models (PREM, Ak135, etc.) and are available at IRIS. At period shorter than about 500 s, and the record duration of about 10 000 s, the synthetics computed with the two methods agree very closely. The AxiSEM synthetics are referred to 'AxiSEM' in this paper. Since we do not know the details of the source time history and we are primarily interested in the long-period characteristics longer than 125 s, we use a source function given by $w(t) = \frac{1}{2T_0}(1 + \cos\frac{\pi t}{T_0}) \quad |t| \le T_0$ and $= 0$ elsewhere. This source is denoted by sf_c_T_0, where T_0 is the source group delay time, or the centroid time of the source.

Fig. 4 compares the synthetic strain records computed for three source models (sf_c_55, sf_c_75 and sf_c_95) with the observed. Since the timing of the original record was calibrated on 1960 June 4, it is believed to be accurate. In Fig. 4, the observed and synthetic records are aligned at the origin time of the event (i.e. 1960 June 6, 05:55:49.1UT). In general, the agreement of the waveform (the amplitude and phase) is good indicating that the assumed mechanism A-1 is compatible with the ISA record. The synthetics filtered with a long time constant, sf_c_95, can match the overall waveform and group delay of G and Rayleigh waves. Fig. 5(a) compares the entire wave train including G1, R1, G2 and R2, and Fig. 5(b), the details of S, G1 and R1 wave trains. Fig. 5(a) shows that the observed record has some spiky high-frequency components suggesting that the event had some irregular motion. The seismic moment estimated from the filtered record is 4.5×10^{20} N·m (M_w = 7.7). The large disparity between M_w (=7.7) and M_s (=6.9) clearly suggests that the June 6 event is an anomalously slow earthquake with enhanced long-period energy and long source duration as suggested by Kanamori & Stewart (1979) with only limited data.

The very long source duration, however, causes some ambiguity in interpretation of the polarity (i.e. phase). As shown in Fig. 5(b), on a plot of S, G1 and R1 with extended timescale without delay, the overall agreement of S, G1 and R1 between the observed and synthetic records is good, supporting the polarity given by A-1.

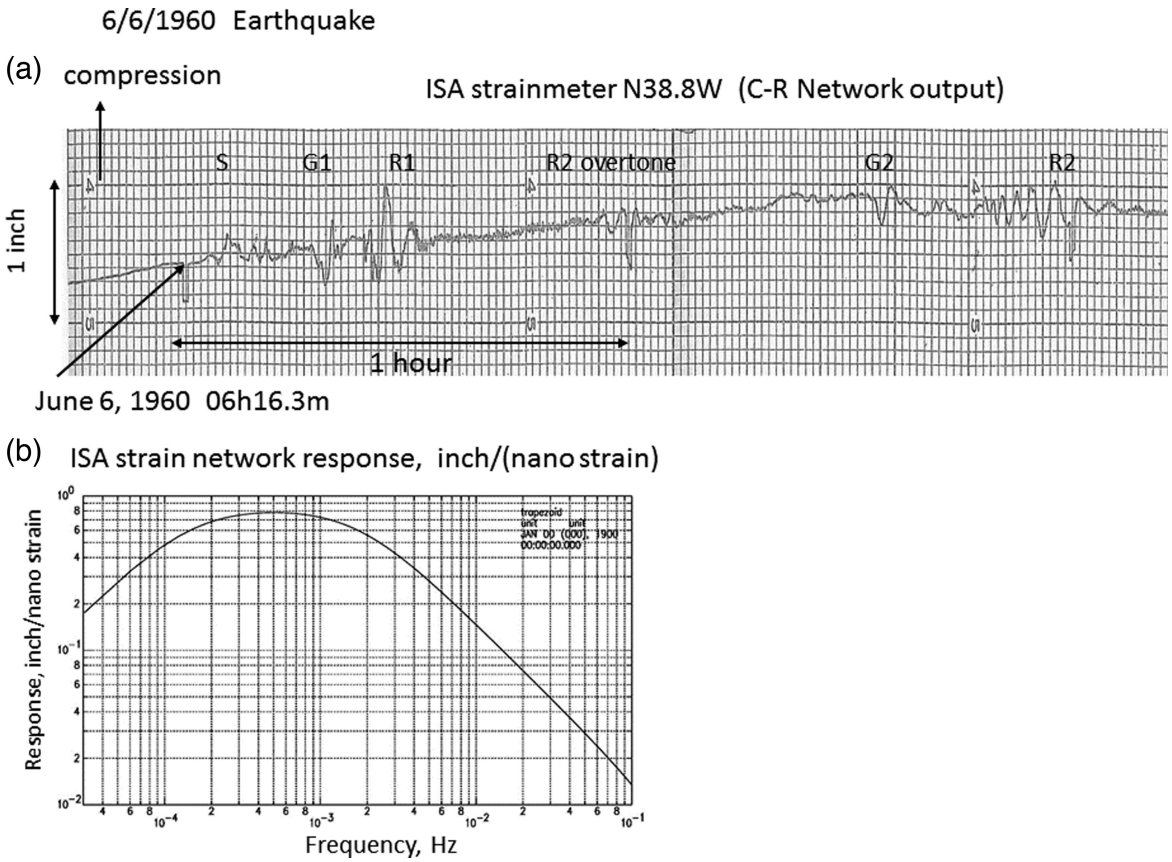

Figure 3. (a) The strain seismogram of the 1960 June 6 earthquake recorded at Isabella (ISA), California. The strain-rod orientation is N38.8°W and the output is passed through the CR network given by Benioff (1963). (b) The strainmeter network is calibrated with earth tide, and the response is given in inch per nanostrain.

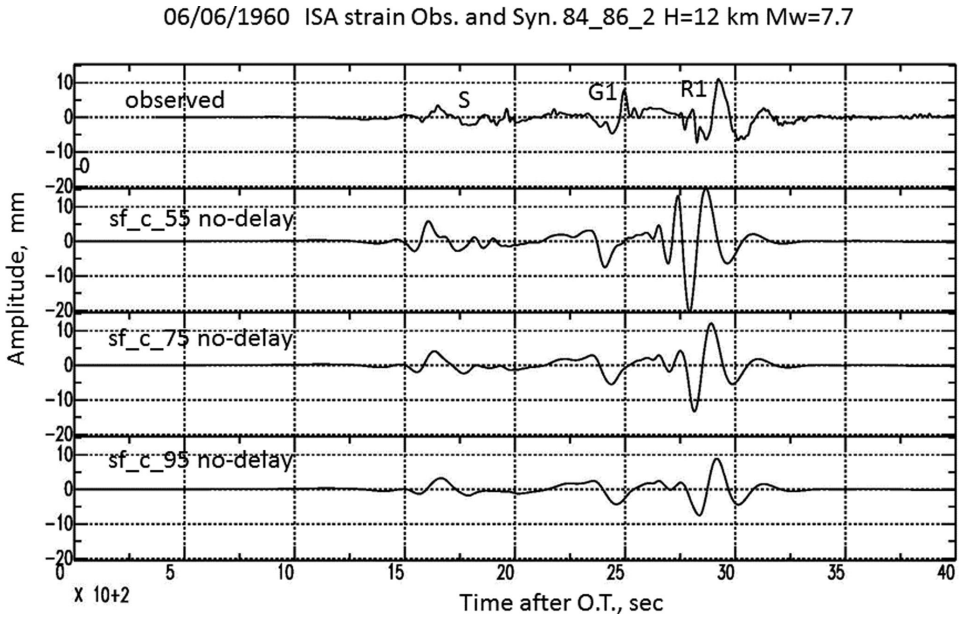

Figure 4. Comparison of the observed and synthetic seismograms (AxiSEM) computed for three sources of the 1960 June 6 earthquake. (Mechanism: s/d/r = 84°/86°/2°, depth: 12 km and moment: 4.5×10^{20} N·m; $M_w = 7.7$.)

However, if the source duration is very long so that an arbitrarily large source group delay is allowed, we can match the waveforms nearly as good by reversing the polarity and delaying the synthetic record by + 100 s, as shown in Figs 6(a) and (b). Thus, the decision on polarity has some ambiguity. Here, on the basis of the better fit of non-dispersive *S* wave without the large group delay, we prefer the A-1 mechanism, but retain the mechanism with the opposite polarity as a viable solution. The polarity of the mechanism used

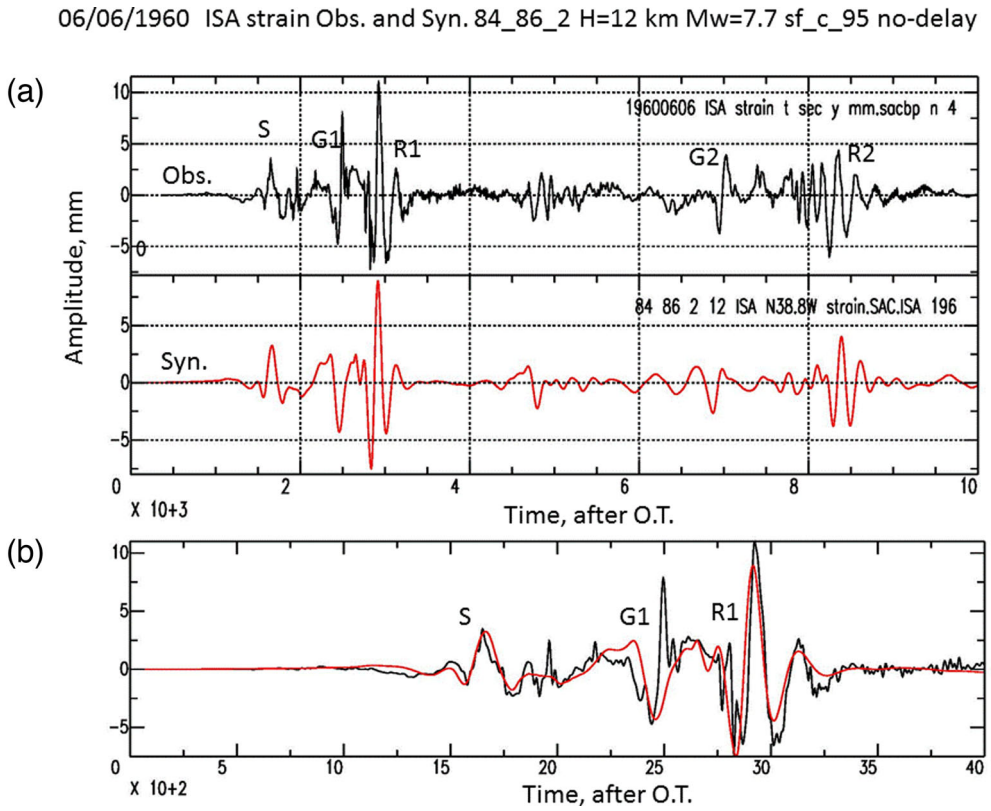

Figure 5. (a) Comparison of the observed strain record (after the long-period trend has been removed) and the strain record computed for the A-1 mechanism. The synthetic record (AxiSEM) is convolved with the filter sf_c_95 to match the group arrival time of the wave train. (b) Blow up of the first 4000 s. Black and red curves show the observed and the synthetic records, respectively.

by Kanamori & Stewart (1979) is almost opposite to A-1, but the polarity chosen by Kanamori & Stewart was ambiguous.

In our synthesis of waveforms, we use a depth of 11 km following the GCMT solution for the 2007 April 21, event. However, the synthetic waveforms at long period are not sensitive to the depth. Fig. 7 shows the synthetics computed for three source depths. Although the synthetic computed for the depth of 11 km matches the observed waveform (shown in Fig. 4) best, it would be possible to modify the mechanism slightly to obtain a better match for deeper models. Thus, the June 6 event can be considerably deeper than 11 km. Fig. 7 includes a synthetic waveform computed for the NDC mechanism AM-1 which displays too large long-period motion at about 2500 s. However, the difference is subtle.

3 UNCERTAINTY IN MECHANISM

We show above that the A-1 mechanism can match the ISA strain record very well, but with a single-station record the solution is not unique. To gain some insight, we explore other solutions in trial-and-error manner as follows. From the ISA record, we can constrain the radiation pattern ratio G/R at long period. Here, the radiation pattern ratio is defined by the source radiation pattern ratio that explains the observed G/R on the ISA strain record. To explain the observed waveform, $1.8 \leq |G/R| \leq 3.5$. With this constraint, we grid search over the parameter space $0 \leq$ (strike, s) $\leq 360^\circ$, $0 \leq$ (dip, d) $\leq 90^\circ$ and $0 \leq$ (rake, r) $\leq 360^\circ$ with 1° step to find the combinations (s/d/r) that can satisfy the constraints. Interestingly, dip-slip mechanisms similar to that of the May 22 $M_w = 9.5$ main shock like s/d/r $= 10^\circ/17^\circ/90^\circ$ and $10^\circ/17^\circ/110^\circ$ can also satisfy the amplitude constraint. Fig. 8 shows the mechanisms and the radiation patterns for these models. To distinguish these models, we can use the IGY long-period seismograms at TSK, Japan. As shown in Fig. 8, TSK is located almost on the node of Rayleigh wave radiation pattern for the A-1 mechanism, while it is located close to the node of G wave for the s/d/r $= 10^\circ/17^\circ/110^\circ$ mechanism. Thus, the A-1 mechanism must yield a large G/R ratio, while the s/d/r $= 10^\circ/17^\circ/110^\circ$ mechanism, a small G/R ratio. Although the quality of the TSK record is marginal, G1 is obviously much larger than R1 as shown in Fig. 9. Comparison of the observed record with the synthetics for the A-1 mechanism and the s/d/r $= 10^\circ/17^\circ/110^\circ$ mechanism clearly shows that the s/d/r $= 10^\circ/17^\circ/110^\circ$ model is not compatible with the TSK observation.

To further explore the range of viable mechanism, we perform another grid search by adding constraints on the initial phase. The constraints used are $1.8 \leq |G/R|_{ISA} \leq 3.5$, $4 \leq |G/R|_{TSK} \leq 30$, $\varphi_{R,ISA} \approx \pi$ and $\varphi_{G,ISA} \approx 0$. Since the NNA record is noisy and small, we apply only a very weak constraint, $0 \leq |G/R|_{NNA} \leq 100$. The initial phases are chosen so that the synthetic waveform for ISA is compatible with the observation. Fig. 10 shows allowable mechanisms by dots on a strike versus rake diagram for eight ranges of dip angle, 0°–15°, 15°–25°, 25°–35°, 35°–45°, 45°–55°, 55°–65°, 65°–75° and 75°–90°. The range of strike, rake and dip includes all the possible mechanisms including the conjugate mechanisms. The panels I to VII indicate that the rake angle is close to 160°–200° or 360°. This means that one nodal plane of the allowable mechanisms is nearly vertical (dip $> 71^\circ$) (eq. 6 of Jarosch & Aboodi 1970), but the dip angle of the auxiliary plane is poorly constrained. The constrained near-vertical nodal plane means that panel VIII ($75^\circ <$ dip $\leq 90^\circ$) alone is sufficient to show all the possible mechanisms. We can identify five groups, (1), (2), (3), (4) and (5), on panel VIII (Fig. 11a),

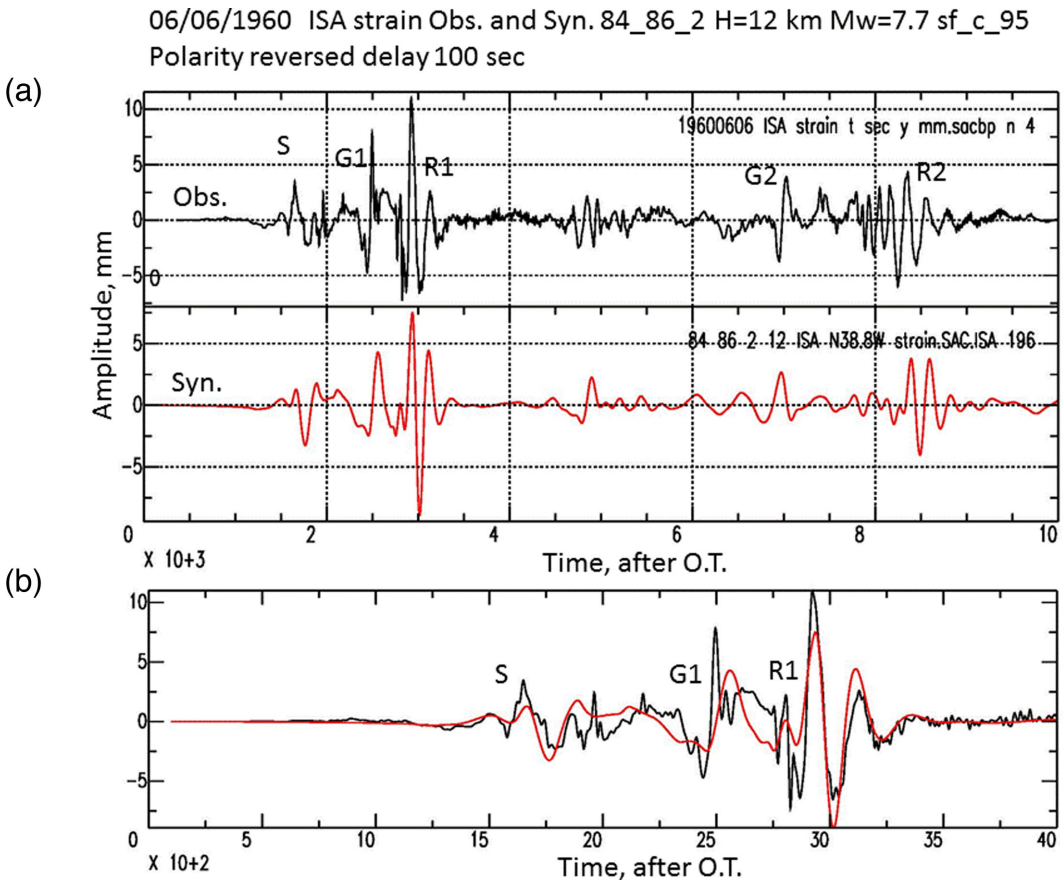

Figure 6. Similar to Fig. 5. The computed trace is reversed in polarity and delayed by 100 s in addition to the group delay of the filter.

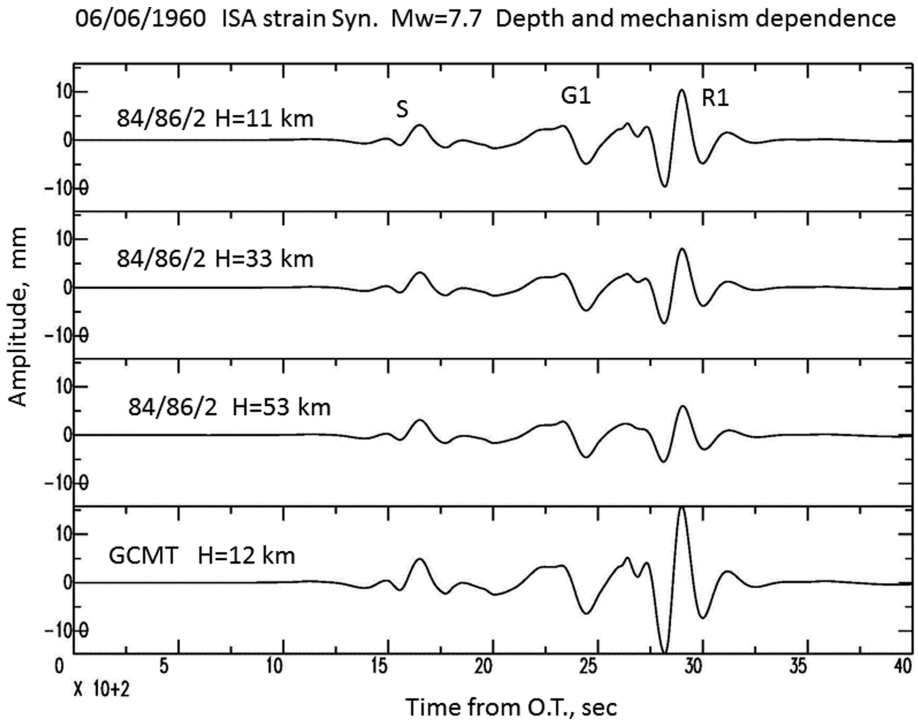

Figure 7. Top three traces: synthetic waveforms computed for A-1 mechanism and three different depths, 12, 33 and 53 km. Bottom trace: the synthetic waveform computed for AM-1 mechanism.

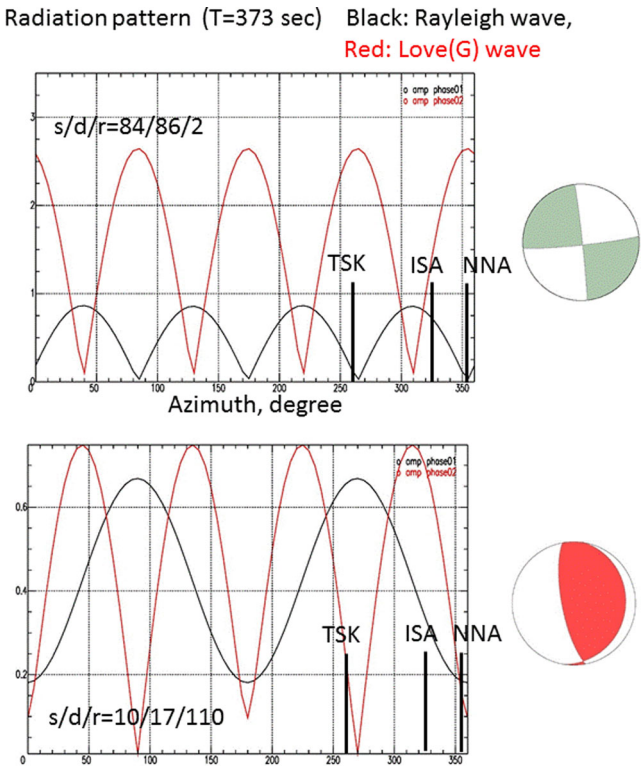

Figure 8. The mechanisms and Love (G, red) and Rayleigh (black) wave amplitude radiation patterns for the A-1 mechanism and a thrust mechanism s/d/r/10°/17°/110°. The azimuths of three stations TSK, ISA and NNA are indicated.

each including many mechanisms. Fig. 11(b) shows representative mechanisms from each group. With the data currently available to us, we cannot constrain the mechanism any further. Thus, all the mechanisms shown on Fig. 11(a) are viable. Group 5 has much fewer events than the other groups (Fig. 11a), and its representative mechanism is a very low-angle strike-slip as shown in Fig. 11(b). This type of mechanism is not commonly observed. If we restrict the dip angle of the auxiliary nodal plane to be larger than 35°, then Group 5 is eliminated as shown in Fig. 11(c). Group 3 is interesting because its east-dipping fault plane is similar to that of the $M_w = 9.5$ main shock. The mechanism A-1 (s/d/r = 84°/86°/2°) represents Group 1. Although we cannot uniquely determine the mechanism, Fig. 11(b) shows that it is primarily right lateral on the NS striking nodal plane, or left lateral on the EW striking nodal plane. These mechanisms are in general similar to the nine GCMT mechanisms of the events in the Aysén region shown in Fig. 2. We use the mechanism A-1 as a representative mechanism.

Kanamori & Stewart (1979) noted the amplitude ratios G3/R3 and G4/R4 recorded with the Pasadena Press–Ewing seismograph as 2.2 and 2.5, respectively. Fig. 12 compares the Press–Ewing seismograms at PAS computed for the A-1 mechanism, which give the corresponding ratios, 2.6 and 2.6. Given, the uncertainty in the source depth, source spectrum, attenuation along the path and calibration of the Press–Ewing seismograph, we consider this agreement satisfactory.

As a final check, we compare the direct strain record for NNA with the synthetics computed for the A-1 and AM-1 mechanisms as shown in Fig. 13. This is a small analogue record with poor quality, but we calibrate it using the tide. Long-period G2, G3, R2 and R3 are barely above the noise level. The PP amplitude of the observed G2 is about three nanostrain that is comparable to that of G2 computed for A-1 and AM-1. The amplitude of the observed R3 appears to be somewhat larger than the computed, but it is possible that for such a long propagation path of R3, the off-great circle energy may have contributed to the nodal amplitude of R2. The AM-1 model yields a larger R/G ratio than A-1, and may be more compatible with the data, but the difference between A1 and AM-1 is marginal.

4 DISCUSSION AND CONCLUSIONS

We could reduce the uncertainty in the source characteristics of the 1960 June 6, slow earthquake in Chile using the newly found well-calibrated ISA strain seismogram with good long-period response. Considering the recent quantitative studies by many investigators in the Aysén Fjord area with modern instrumentation and the GCMT

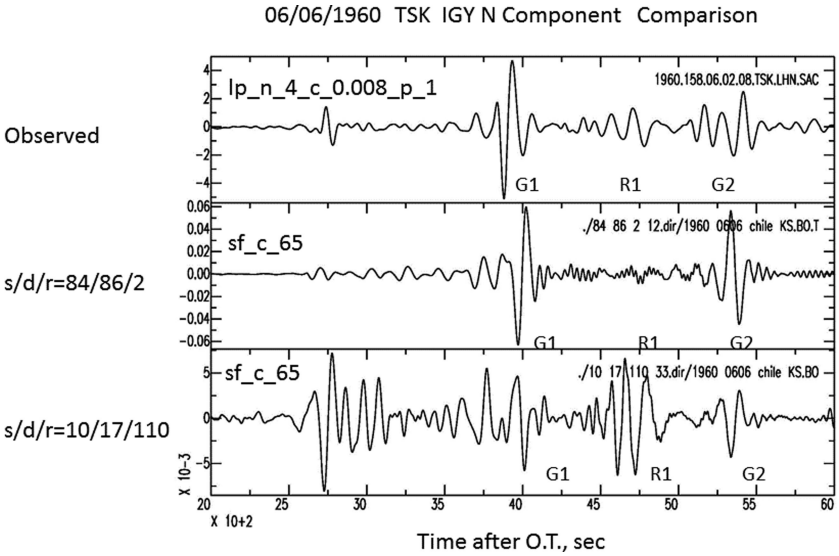

Figure 9. Comparison of the observed TSK record with the corresponding synthetics computed for the A-1 and a dip-slip (s/d/r = 10°/17°/110°) mechanism. The amplitude ratio G1/R1 of the A-1 synthetic is more compatible with the observed ratio than that for the dip-slip model. Observed and synthetic records are filtered so that the surface waves are displayed with about the same period.

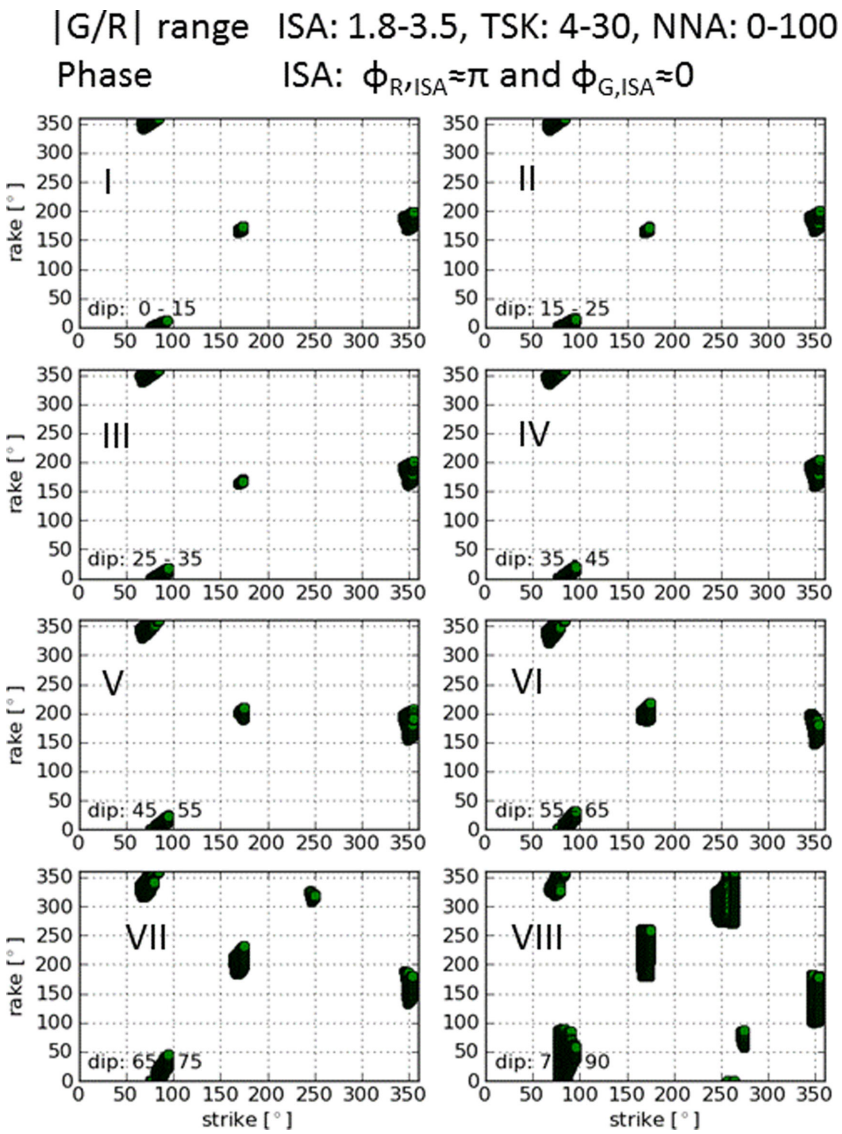

Figure 10. Allowable s/d/r for the constraints $1.8 \leq |G/R|_{ISA} \leq 3.5$, $0 \leq |G/R|_{NNA} \leq 100$, $4 \leq |G/R|_{TSK} \leq 30$, $\varphi_{R,ISA} \approx \pi$ and $\varphi_{G,ISA} \approx 0$. Panels I to VIII show rake versus strike diagrams for eight dip angle ranges. Dark clusters show the regions of acceptable s/d/r.

catalogue, we conclude that the mechanism of the June 6 event is most likely similar to that of the largest event during the 2007 Aysén earthquake swarm (A-1, s/d/r = 84°/86°/2°), although with the limited data we have, we cannot completely eliminate other possibilities.

The seismic moment, $M_0 = 4.5 \times 10^{20}$ N·m, is nearly 160 times larger than that of the 2007 April 21, Aysén event. The long duration of the source (at least about 190 s) and the large M_w–M_s disparity (7.7 versus 6.9) confirm that the June 6 event is an unusually slow earthquake. Unlike for the 2007 sequence, no reports of extensive swarms and landslides were found for the 1960 June 6 event despite its much larger M_w. We could not determine the depth very well, but the slowness of the event suggests that it could be deeper than the 2007 sequence; it may have occurred in a less brittle environment, resulting in relatively minor shallow macroseismic effects. The very slow slip may be an indication of high-temperature ductile fault-zone property caused by the slab gap associated with the subduction of the Chile Rise as suggested by Russo *et al.* (2010). With the large M_w and large slip budget, it represents a major tectonic event in this region.

A possible tectonic structure in the area that can accommodate such a large event is the LOF. Cembrano *et al.* (1996) state that the LOF zone may be a long-lived shear zone that accommodated continental-scale deformation arising from the Nazca-South America plate convergence, but regional-scale offset markers are unknown. The recent seismic activity has been relatively low, but Lange *et al.* (2008) observed 75 shallow crustal events with $M_w < 3.5$ along a 130 km long segment of the LOF zone during an 11 month period. The most notable recent activity was the 2007 Aysén swarm. Most investigators have associated the 2007 Aysén swarm with the LOF together with the subduction of the Chile Rise. If the 1960 June 6 event occurred on the LOF, its large seismic moment represents a major slip budget of this fault. Wang *et al.* (2007) found evidence for the active dextral shear motion of the LOF zone which can be described as block translation at 6.5 mm yr^{-1}.

It is interesting that the June 6 event occurred during the aftershock sequence of the May 22, $M_w = 9.5$, Chilean earthquake on the Nazca-South American subduction plate boundary. The large moment of the June 6 event suggests significant interaction between the megathrust boundary and the LOF. The interaction and

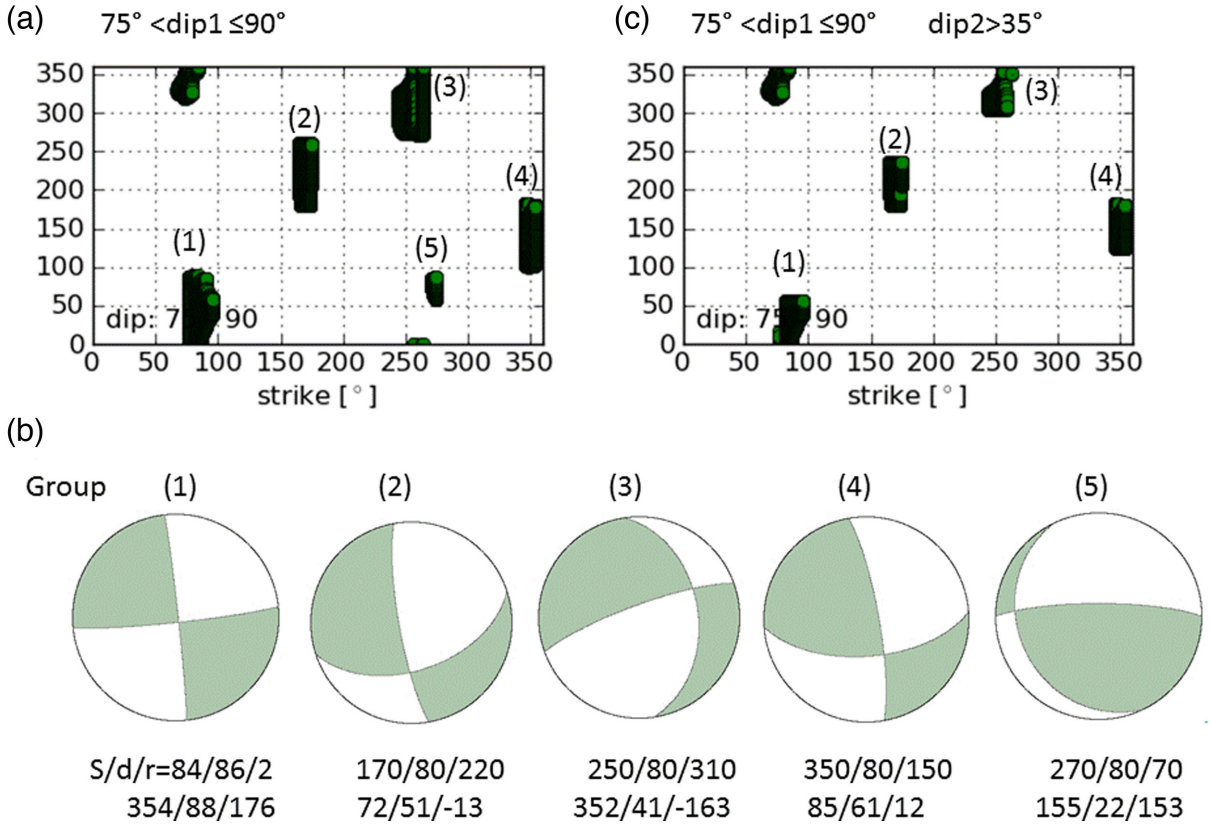

Figure 11. (a) Five groups shown on panel VIII of Fig. 10. (b) Representative mechanisms for each group. (c) Similar to Fig. 11(a). Only the mechanisms for which the dip of the auxiliary plane is larger than 35° are included to remove the mechanism like Group 5 in Fig. 11(b).

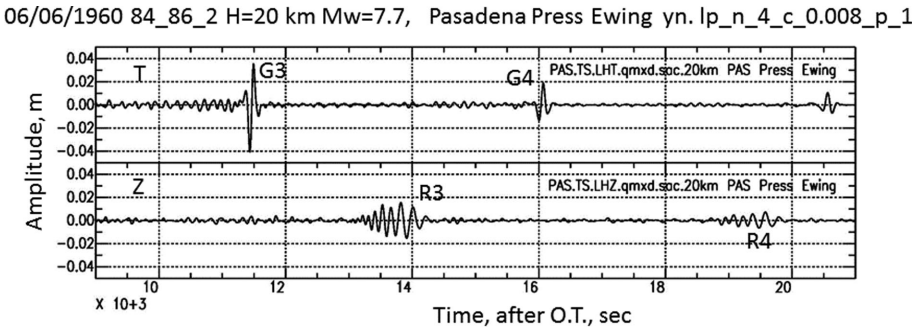

Figure 12. Synthetic PAS Press–Ewing seismograms computed with A-1 mechanism. A generic response with pendulum period 30 s, galvanometer period 90 s and magnification 2300 is used.

slip partitioning between a megathrust and an upper plate strike-slip fault has been a subject of extensive study (e.g. Fitch 1972). The examples are seen in Sumatra, Nankai trough, and the Philippines; the case for the Nazca-South America plate boundary and the LOF may be a case with very strong interaction.

The occurrence of aftershocks is often discussed in terms of Coulomb stress caused by a main shock. Following Fitch (1972), if we use a simple geometry for the $M_w = 9.5$ 1960 May 22, Chilean main shock and the, 1960 June 6, aftershock shown in Fig. 14(a), we can see qualitatively that a large pure megathrust earthquake on the subduction boundary unclamps the right-lateral target fault because the normal stress on the target fault decreases but the shear stress changes little. This can be more quantitatively illustrated in Fig. 14(b), where the Coulomb stress change on the target fault computed with the Coulomb 3.3 Software (Toda *et al.* 2011) is shown. The megathrust main shock is modelled with a 800 × 200 km^2 rectangular fault with a dip = 17° and uniform slip of 34 m ($M_w = 9.5$ with rigidity = 40 GPa). The LOF is modelled as a vertical right-lateral fault parallel to the megathrust at a distance of 200 km from the trench. The figure shows that the right-lateral Coulomb stress at a depth of 10 km is about + 0.7 MPa (unclamping) for a coefficient of friction of 0.4, favouring a right-lateral slip on the LOF.

Our choice of the NS striking right-lateral fault is strongly influenced by the proximity of the June 6 event to the LOF. From the waveform alone and the first-motion data (e.g. fig. 3 of Kanamori & Stewart 1979), an EW trending right-lateral fault cannot be completely ruled out, as discussed earlier. To see the effect of Coulomb stress on such a fault, we test another target fault shown in Fig. 14(c). As shown in Fig. 14(d), the Coulomb stress on the fault plane is

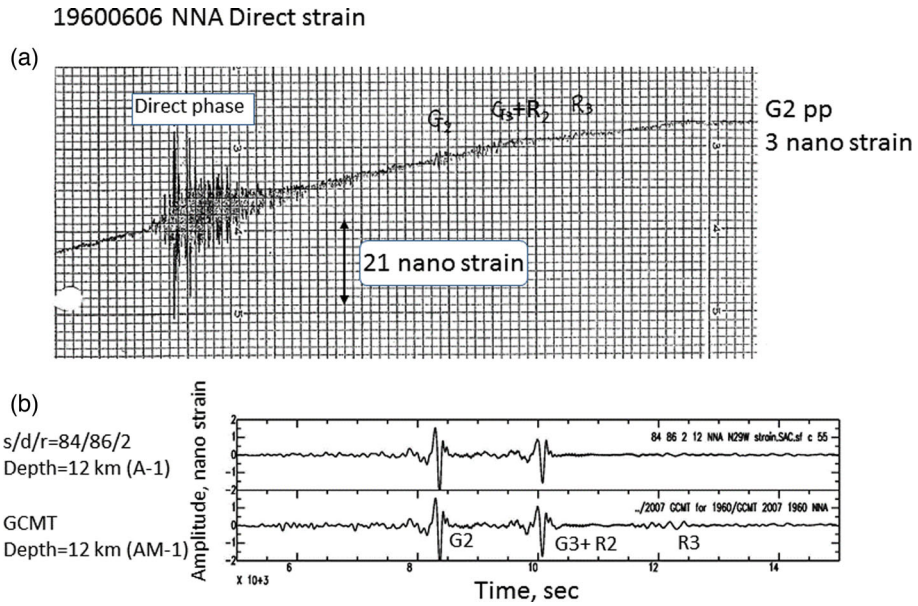

Figure 13. Comparison of NNA direct strain record with those computed for A-1 and AM-1. The strain record is calibrated by tide.

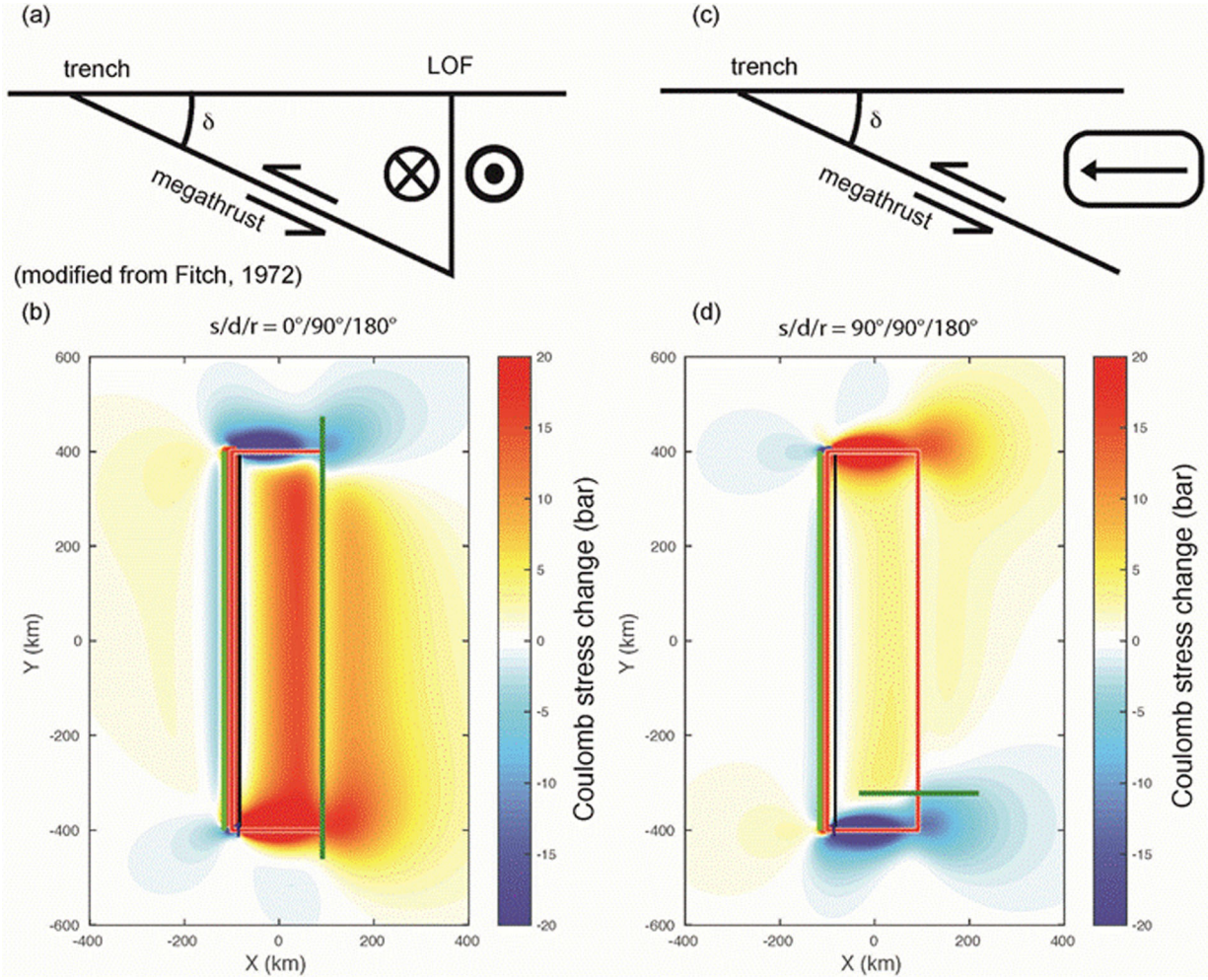

Figure 14. (a) A simple geometry of the Chilean megathrust and the LO fault following the simple plate boundary model of Fitch (1972). (b) Coulomb stress computed for an $M_w = 9.5$ Chilean earthquake fault model (black rectangle, dip $= 17°$, $S = 800 \times 200$ km^2 and slip $= 34$ m), and the location of the LO fault (green line). (c) Geometry of an EW trending right-lateral target fault. (d) Coulomb stress computed for an EW trending right-lateral target fault (green line). The Coulomb stress at a depth of 10 km on the target fault is computed with Coulomb 3.3 Software (Toda *et al.* 2011).

also positive but much smaller than that for the geometry shown in Fig. 14(a). Thus, at face value, we can conclude that the LOF geometry is preferred, if the June 6 event was triggered by the Coulomb stress caused by a thrust fault model for the 1960 Chilean main shock.

We note, however, that many other factors can affect the aftershock activity. First, dynamic stress from such a large megathrust can be more significant than the static Coulomb stress. Although we do not have direct data for the 1960 Chilean earthquake, for the somewhat smaller 2011 Tohoku-Oki, Japan, earthquake (M_w = 9.0), Midorikawa *et al.* (2012) reported that the average ground-motion velocity at a fault distance (distance normal to the fault) of 100 km was about 0.3 m s^{-1} which corresponds to a dynamic stress change of about 3 MPa, significantly larger than the Coulomb stress. Second, the details of the mechanism and the slip distribution of the Chilean main shock are not well determined. For example, the slip models obtained by Barrientos & Ward (1990) and Moreno *et al.* (2009) from geodetic data indicate much smaller slip to the south than in the north. Also, the plate convergence direction in south Chile has some right-lateral component along the trench axis. If we include this effect in the Coulomb stress computation, it will decrease the right-lateral Coulomb stress on the LOF fault.

Given the large dynamic stress change and the extensive geothermal activities in the Aysén region, dynamic triggering can be more important than static Coulomb stress in this case. Hill *et al.* (1993) demonstrated extensive dynamic triggering in several geothermal areas after the 1992 Landers, California, earthquake.

No reports on macroseismic effects of the June 6 event are available to us. This is surprising, given the extensive landslides and tsunamis reported for the 2007 swarm events with much smaller magnitudes. It is possible that the slowness and somewhat larger depth of the June 6 event may have limited its macroseismic effects.

ACKNOWLEDGEMENTS

Dr Stewart Smith kindly sent us the original ISA strip-chart record of the 1960 May 22, M_w = 9.5 earthquake, which he has carefully kept in good condition. Availability of this record is the impetus to our study which almost entirely depends on this invaluable record. Dr Guy Masters provided us with the hand-digitized data of the ISA strain record. Dr Joann Stock introduced us to the literature on the recent investigations on the Aysén swarm. Dr Shingo Watada provided us with the Tsukuba IGY seismograms. We used a program written by Dr Duncan Agnew for computing tidal variations at ISA, California and Ñaña, Peru. Dr Sergio Barrientos provided us with the information on the 1960 June 6, event. We used Syngine web service at the Data Management Center of Incorporate Research Institutions for Seismology for computing some of the synthetic seismograms. We thank the two anonymous reviewers for their careful review.

REFERENCES

Agurto, H., Rietbrock, A., Barrientos, S., Bataille, K. & Legrand, D., 2012. Seismo-tectonic structure of the Aysén Region, Southern Chile, inferred from the 2007 M_w = 6.2 Aysén earthquake sequence, *Geophys. J. Int.*, **190**, 116–130.

Barrientos, S.E. & Ward, S.N., 1990. The 1960 Chile earthquake: inversion for slip distribution from surface deformation, *Geophys. J. R. astr. Soc.*, **103**, 589–598.

Benioff, H., 1962. Movements on major transcurrent faults, in *Continental Drift*, pp. 103–134, ed. Runcorn, S.K., Academic Press, London.

Benioff, H., 1963. Source wave forms of three earthquakes, *Bull. seism. Soc. Am.*, **53**, 893–903.

Benioff, H., Press, F. & Smith, S., 1961. Excitation of the free oscillations of the Earth by earthquakes, *J. geophys. Res.*, **66**, 605–619.

Cembrano, J., Hervé, F. & Lavenu, A., 1996. The Liquiñe Ofqui fault zone: a long-lived intra-arc fault system in southern Chile, *Tectonophysics*, **259**, 55–66.

Chinn, D.S. & Isacks, B., 1983. Accurate source depths and focal mechanisms of shallow earthquakes in western south America and in the New Hebrides island arc, *Tectonics*, **2**, 529–563.

Cifuentes, I.L., 1989. The 1960 Chilean earthquakes, *J. geophys. Res.*, **94**, 665–680.

Comte, D., Gallego, A., Russo, R., Mocanu, V., Murdie, R. & VanDecar, J., 2007. The Aysen (Southern Chile) 2007 seismic swarm: volcanic or tectonic origin?, in *EOS, Trans. Am. geophys. Un.,* **88**(23), Jt. Assem. Suppl., Abstract S43C-04.

Dziewonski, A.M. & Anderson, D.L., 1981. Preliminary reference Earth model, *Phys. Earth planet. Inter.*, **25**, 297–356.

Fitch, T.J., 1972. Plate convergence, transcurrent faults, and internal deformation adjacent to southeast Asia and western Pacific, *J. geophys. Res.*, **77**, 4432–4460.

Gutenberg, B. & Richter, C.F., 1954. *Seismicity of the Earth and Associated Phenomena*, 2nd edn, Princeton Univ. Press.

Hill, D.P. *et al.*, 1993. Seismicity remotely triggered by the magnitude 7.3 Landers, California, earthquake, *Science*, **260**, 1617–1623.

Kanamori, H. & Stewart, G.S., 1979. A slow earthquake, *Phys. Earth planet. Inter.*, **18**, 167–175.

Jarosch, H. & Aboodi, E., 1970. Towards a unified notation of source parameters, *Geophys. J. R. astr. Soc.*, **21**, 513–529.

Lange, D., Cembrano, J., Rietbrock, A., Haberland, C., Dahm, T. & Bataille, K., 2008. First seismic record for intra-arc strike-slip tectonics along the Liquiñe-Ofqui fault zone at the obliquely convergent plate margin of the southern Andes, *Tectonophysics*, **455**, 14–24.

Legrand, D., Barrientos, S., Bataille, K., Cembrano, J. & Pavez, A., 2011. The fluid-driven tectonic swarm of Aysen Fjord, Chile (2007) associated with two earthquakes (M_w = 6.1 and M_w = 6.2) within the Liquiñe-Ofqui Fault Zone, *Cont. Shelf Res.*, **31**, 154–161.

Midorikawa, S., Miura, H. & Atsumi, T., 2012. Strong motion records from the 2011 off the Pacific coast of Tohoku earthquake, in *International Symposium on Engineering Lessons Learned from the 2011 Great East Japan Earthquake*, pp. 297–304, ed. Kawashima, K., Japan Association for Earthquake Engineering (Tokyo), Tokyo, Japan.

Moreno, M.S., Bolte, J., Klotz, J. & Melnick, D., 2009. Impact of megathrust geometry on inversion of coseismic slip from geodetic data: application to the 1960 Chile earthquake, *Geophys. Res. Lett.*, **36**, L16310, doi:16310.11029/12009GL039276.

Naranjo, J.A., Arenas, M., Clavero, J. & Munoz, O., 2009. Mass movement-induced tsunamis: main effects during the Patagonian Fjordland seismic crisis in Aisen (45°25′S), Chile, *Andean Geol.*, **36**, 137–145.

Nissen-Meyer, T., van Driel, M., Stähler, S.C., Hosseini, K., Hempel, S., Auer, L., Colombi, A. & Fournier, A., 2014. AxiSEM: broadband 3-D seismic wavefields in axisymmetric media, *Solid Earth*, **5**, 425–445.

Pérez-Flores, P., Cembrano, J., Sánchez-Alfaro, P., Veloso, E., Arancibia, G. & Roquer, T., 2016. Tectonics, magmatism and paleo-fluid distribution in a strike-slip setting: insights from the northern termination of the Liquiñe–Ofqui fault System, Chile, *Tectonophysics*, **680**, 192–210.

Rothe, J.P., 1969. *The Seismicity of the Earth 1953–1965*, UNESCO.

Russo, R.M., VanDecar, J.C., Comte, D., Mocanu, V.I., Gallego, A. & Mudie, R.E., 2010. Subduction of the Chile Ridge: upper mantle structure and flow, *GSA Today*, **20**, 4–10.

Sepulveda, S.A. & Serey, A., 2009. Tsunamigenic, earthquake-triggered rock slope failures during the April 21, 2007 Aisen earthquake, southern Chile (45.5°S), *Andean Geol.*, **36**, 131–136.

Sepúlveda, S.A., Serey, A., Lara, M., Pavez, A. & Rebolledo, S., 2010. Landslides induced by the April 2007 Aysén Fjord earthquake, Chilean Patagonia, *Landslides*, **7**, 483–492.

Smith, S.W., 1966. Free oscillations excited by the Alaskan earthquake, *J. geophys. Res.*, **71**, 1183–1193.

Toda, S., Stein, R., Sevilgen, V. & Lin, L., 2011. Coulomb 3.3 Graphic-rich deformation and stress-change software for earthquake, tectonic, and volcano research and teaching – user guide, Open-File Rep. 2011-1060, U.S. Geol. Surv.

Wang, K., Hu, Y., Bevis, M., Kendrick, E., Smalley, R., Vargas, R.B. & Lauría, E., 2007. Crustal motion in the zone of the 1960 Chile earthquake: detangling earthquake-cycle deformation and forearc-sliver translation, *Geochem. Geophys. Geosyst.*, **8**, Q10010, doi:10.1029/2007GC001721.

Woodhouse, J.H., 1988. The calculation of eigenfrequencies and eigenfunctions of the free oscillations of the Earth and the Sun, in *Seismological Algorithms*, pp. 321–370, ed. Doornbos, D.J., Academic Press, New York.

APPENDIX: CALIBRATION OF THE ISA STRAIN SEISMOGRAM

The strain seismogram of the 1960 Chilean earthquake recorded at Isabella has not been completely documented. Fortunately, we have recently obtained two important records: (1) a hand-digitized data starting from 23:56:17.5 (UT), 1960 May 22 to June 9, and sampled at 1 min. The total number of samples is 26 668. This record was kindly provided by Prof Guy Masters. (2) The original long strip-chart record from about 21:00 (UT), 1960 May 27 to June 9, provided by Prof Stewart Smith. This record is the output of a capacitor–resistance (CR) network connected to the Isabella strainmeter. These data together with the direct strain record published in Benioff (1962) allowed us to perform a fairly complete calibration of this record.

The calibration involves the following three steps.

1. On the direct strain record published in Benioff (1962), a gain factor, g1, is indicated as 4.8×10^{-9} inch^{-1}. Since the earth tide is recorded on this strain seismogram, we calibrate it against the theoretical tide computed using a code provided by Duncan Agnew, and obtained a gain factor as 5.6×10^{-9} inch^{-1} (Fig. A1). This value is used throughout this paper.

2. We compare the digitized record against the long strip-chart record obtained through the CR network and confirm that the digitized record was hand digitized from the analogue strip-chart record starting from 23:56:17.5 (UT), 1960 May 22. This time is just after the arrival of G4 and just before the arrival of R4. We could not find the analogue record before 21:00, 1960 May 27. Comparing several distinct features (e.g. G2 wave of the June 6 event) found on both the digitized record and the analogue network record, we estimate the conversion factor (from analogue to digital record), g2, to be 156 counts inch^{-1}.

3. The response of the CR network attached to the Isabella strainmeter was discussed by Benioff (1963) and Smith (1966). However, the response of the specific network used at the time of the 1960 Chilean earthquake is ambiguous. Benioff (1963) shows (Fig. 3) a CR network consisting of two capacitors (C1 = 100 μF and C2 = 100 μF) and two resistors (R1 = 2 MΩ and R2 = 5 MΩ) that was used for the record of Montana earthquake on 1959 August 18. The same CR network was most likely used on 1960 May 22. Smith (1966) showed a graph of the amplitude response curve of the network used for the recording of the 1960 Chile earthquake, but the specific network configuration and constants were not mentioned. The shape of the response curve given by Smith (1966) is very similar to that computed for the CR network given by Benioff (1963) for the period shorter than 2000 s, but is considerably different at period longer than 2000 s. At 1 hr, the response given by Smith (1966) is about 70 per cent of that given by Benioff (1963). Since the shape of the response of the CR network given by Benioff (1963) is very close to that shown by Smith (1966), here we use the CR response for the period shorter than 30 min.

The response of the CR network shown in Benioff (1963) is given by

$$N(\omega) = G\frac{2jh\omega_0\omega}{-\omega^2 + 2jh\omega_0\omega + \omega_0^2}$$

as a function of angular frequency ω where $\omega_0^2 = \frac{1}{C_1R_1C_2R_2}$, $h = \frac{R_1C_1+R_2C_2+R_2C_1}{2\sqrt{C_1R_1C_2R_2}}$ and G is the gain factor at $\omega = \omega_0$. This

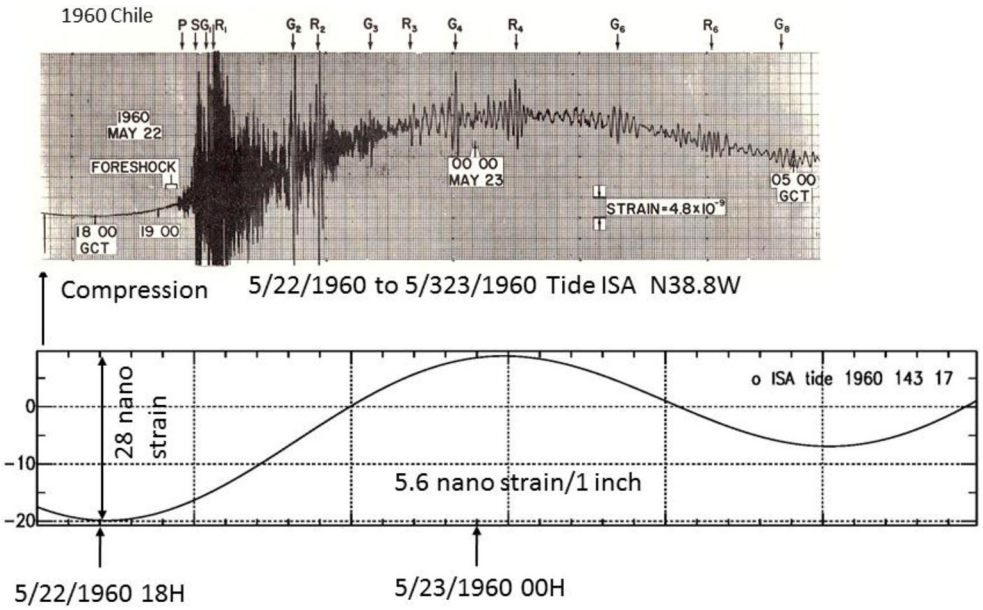

Figure A1. Calibration of the ISA direct strain record. Top: the ISA direct strain record (Benioff 1962). Bottom: computed tide. The record over the time interval from 18:00 1960 May 22 to 00:00 May 23 is used for calibration.

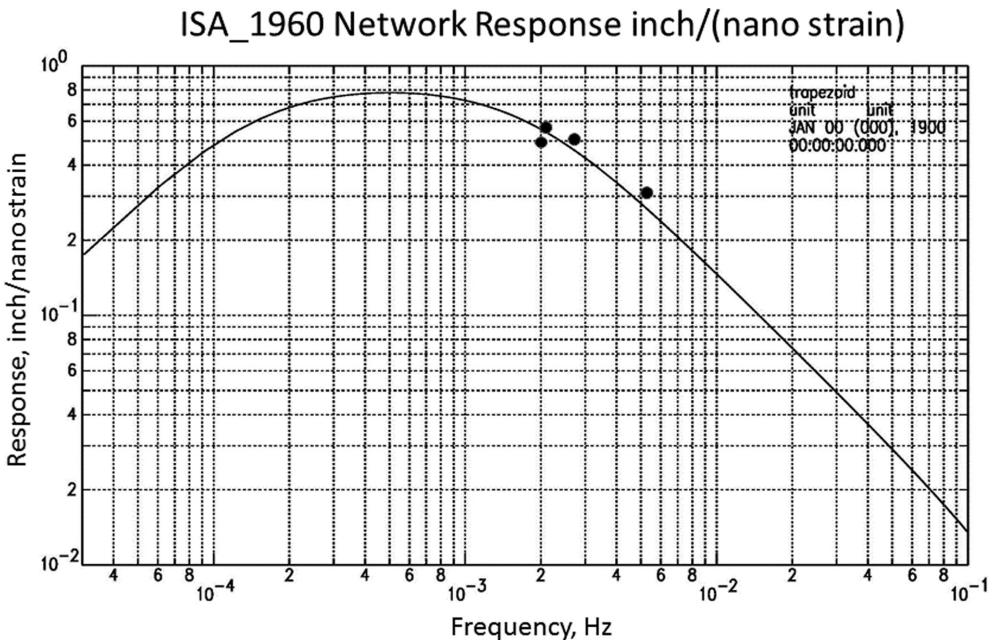

Figure A2. Calibration of the CR network at ISA. The shape of the response curve is determined using the CR circuit constants given in Benioff (1963). The dots show the gain factors estimated from comparisons of the amplitudes of R4, G6, R6 and G8 recorded on both the direct and the network records shown in Fig. A3.

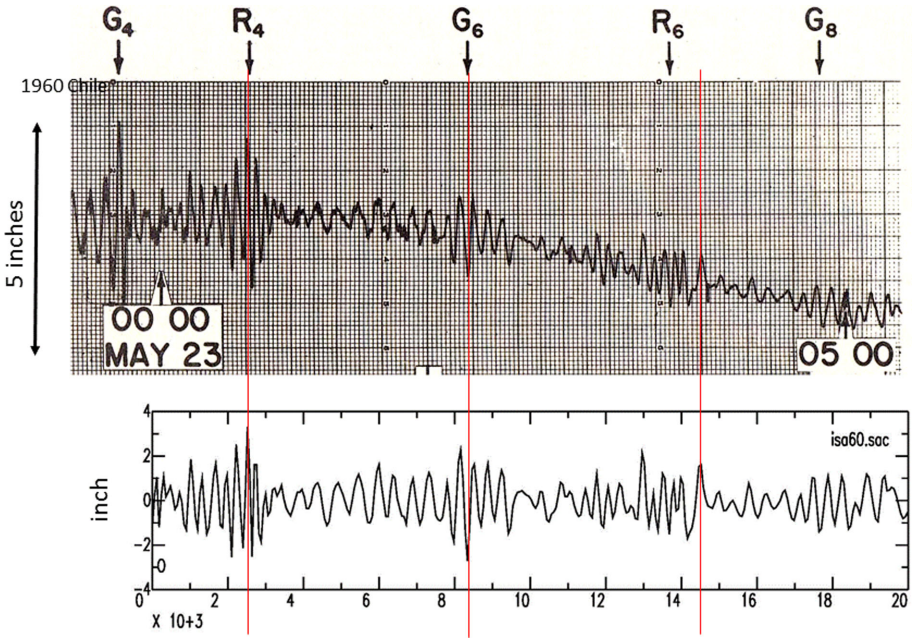

Figure A3. Comparison of the direct (top) and network (bottom) outputs of the ISA strain record. Note the higher gain at long period on the network record than the direct record.

response peaks at $\omega = \omega_0$. In Benioff (1963), fig. 3 shows this response with G = 1. For the given constants (C1 = 100 μF, C2 = 100 μF, R1 = 2 MΩ and R2 = 5 MΩ), $\omega_0^2 = 10^{-5}$ s^{-2} (period is 1987 s = 33 min), and $h = 1.9$. The response curve thus computed is shown by Fig. A2. At this point, the gain factor G at the peak response is not determined

The remaining task is to determine the gain factor G. We determine G using the R4, G6, R6 and G8 phases which are clearly recorded on both the direct and the network records as shown in Fig. A3. The comparison of the amplitude of these phases is shown in Table A1.

Table A1. Comparison of the direct record and network record.

Phase	Period (s)	Amplitude network (inch)	Amplitude direct (nanostrain)	Gain (inch nano-strain^{-1})
R4	218	5.16	18.4	0.28
G6	424	5.12	10.0	0.51
R6	533	3.44	6.2	0.55
G8	497	2.20	4.5	0.49

Notes: The gain factors (column 5) determined for these phases at different periods fix the position of the response curve as shown in Fig. A2. The peak response G is 0.78 inches per nanostrain. Smith's (1966) fig. 3 indicates a gain factor of 2000 counts per nanostrain at the peak, but this seems to be a typographical error.